Supplementary materials

Can Septic-System Management Practices Outweigh Climatic and Anthropogenic Drivers of Phosphorus-induced Lake Eutrophication?

Carmen Iulia Oniga[a], Elmira Hassanzadeh[a,b,*], Dominique Claveau-Mallet[a]

a. Department of Civil, Geological and Mining Engineering, Polytechnique Montréal, Montréal, Québec, Canada

b. United Nations University Institute for Water, Environment and Health (UNU-INWEH), Hamilton, Ontario, Canada

---

[*] Corresponding author. E-mail: elmira.hassanzadeh@polymtl.ca

S1. Lake water quantity-quality modeling

S1.1 Soil characteristics.

Pearson correlation coefficients obtained for the Henry, Freundlich, and Langmuir isotherm models were used to evaluate which model best describes the adsorption behavior of the different soil types based on collected samples surrounding the lake in this watershed. As shown in Fig. S1, the Langmuir isotherm exhibits the highest correlation coefficients, indicating that it provides the best fit to the observed adsorption data. Therefore, the Langmuir model was selected to represent the adsorption behavior, and the corresponding isotherm curves for the six soil types are presented in Fig. S2, the information of which is used to find soil conservation time, explained below.

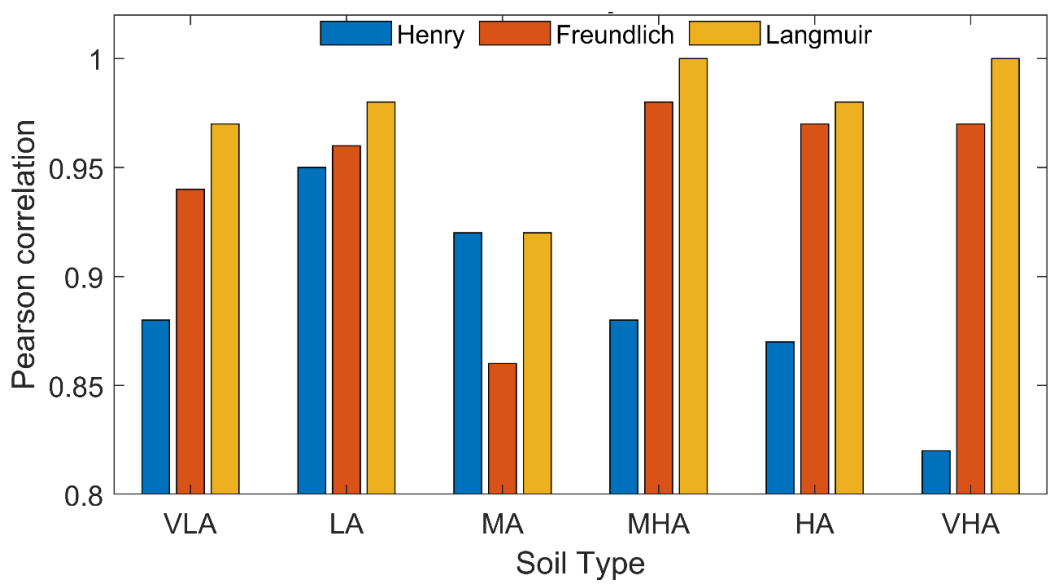

Fig. S1. Pearson correlation (R^2) for sorption isotherms, given six soil types, very low adsorption (VLA), low adsorption (LA), medium adsorption (MA), medium high adsorption (MHA), high adsorption (HA) and very high (VHA) adsorption

To determine the mass of phosphorus reaching the lake, a mass conservation equation is applied between the mass of phosphorus at the exit of the septic system (i.e., at the base of the drain field) and the mass of phosphorus migrating through the soil matrix. The contaminant may transition from the liquid phase to solid phase; however, its total mass remains conserved, as shown in Equations S1–S3.

$$m_{P\ wastewater} = m_{P\ soil} \tag{S1}$$

$$C_p \cdot Q_{eff} \cdot t_{conservation} = V_{soil} \cdot \rho_{soil} \cdot q_{ads} \quad \text{(S2)}$$

$$t_{conservation} = \frac{V_{sol} \cdot \rho_{sol} \cdot q_{ads}}{C_p \cdot (Q_{aff} \cdot OR)} \quad \text{(S3)}$$

where C_p is the P concentration at the base of the drain field after secondary treatment, Q_{aff} is the septic system incoming affluent flow, Q_{eff} is the septic system outcoming effluent flow, $t_{conservation}$ is the P conservation time in the soil, OR is watershed average occupancy rate, V_{soil} is the soil volume solicited for P transport, ρ_{soil} is the soil density of 1800 kg/m^3, and q_{ads} is the soil's P adsorption capacity.

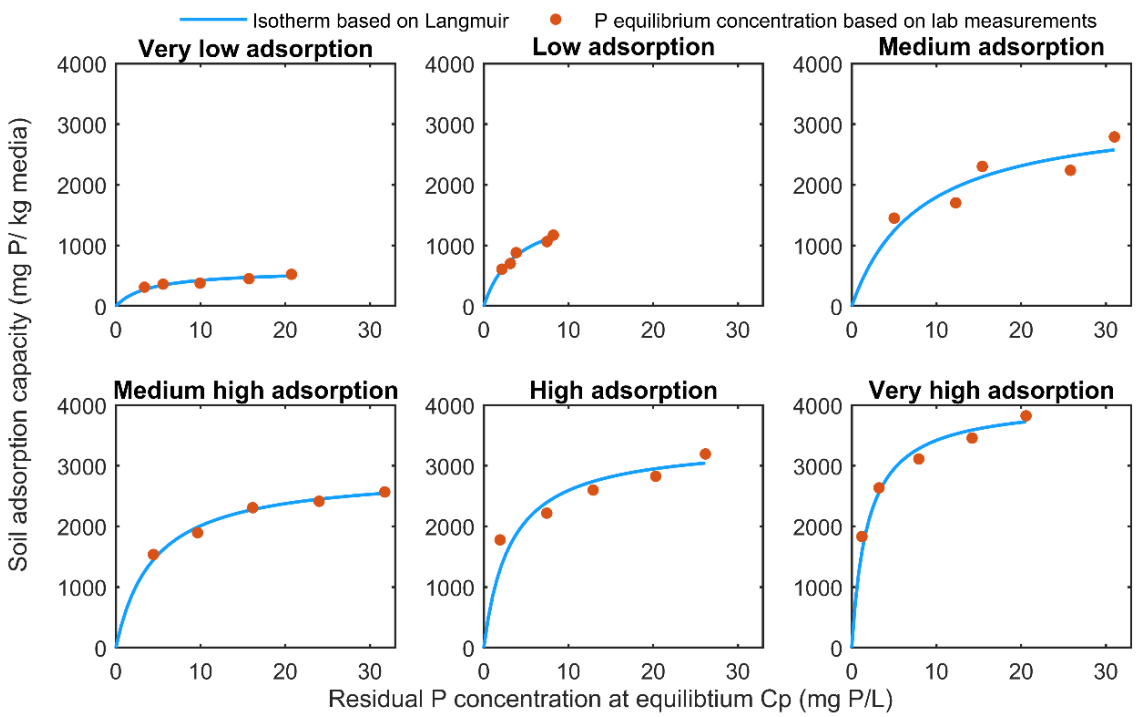

Fig. S2. Isotherm curves constructed based on estimated sorption capacity and residual phosphorus concentration for tested soil samples surrounding lake

The adsorption capacity q_{ads} is determined based on the isotherm curves, C_p represents the P concentration that leaves the septic system, i.e., at the base of the drain field after wastewater was treated in mg P/L. C_p on the abscissa allows to determine q_{ads} on the y-axis for every isotherm shown in Fig. S2. For instance, case CSS15 yields a P concentration C_p of 3.80 mg P/L at the exit of the septic system which, if read on the abscissa and followed along the y-axis until it intersects

the isotherm curve of VLA soil type for instance, the corresponding q_{ads} is 291 mg P/ kg of substrate. Fig. S3 shows these values for eight conformity cases and sorption capacity.

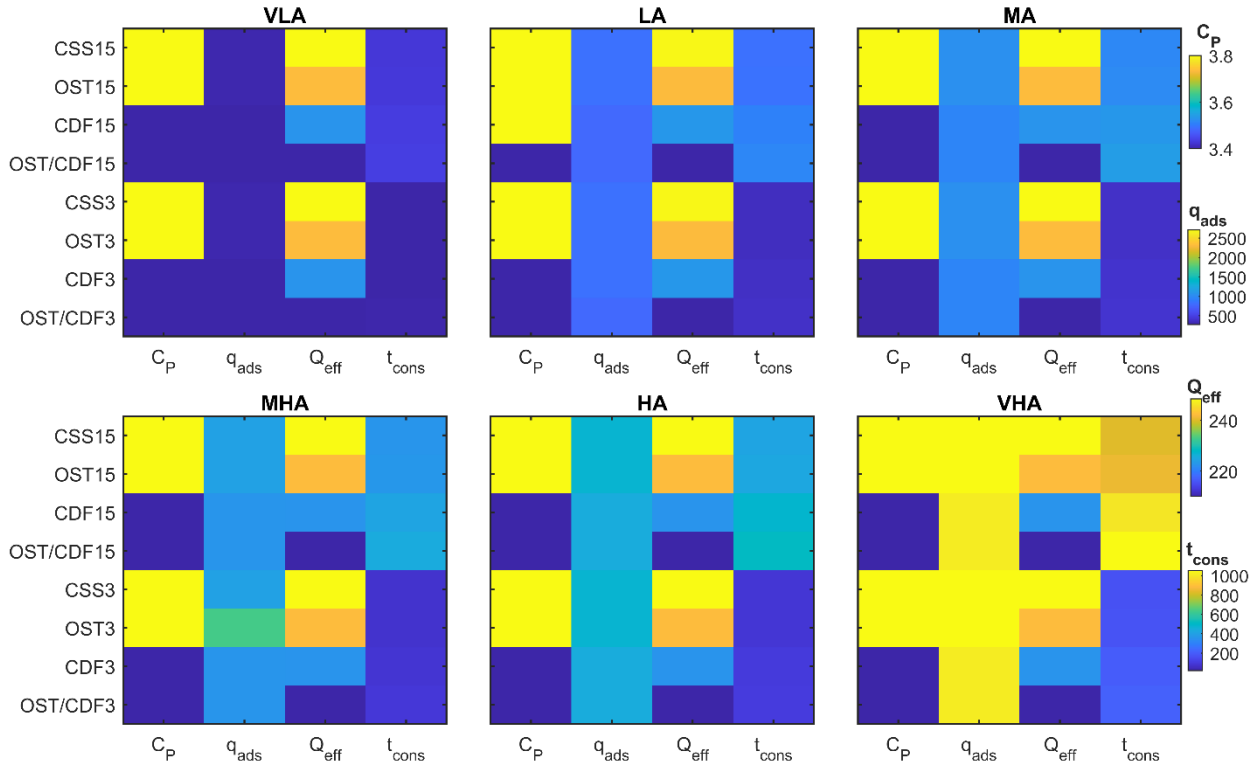

Fig. S3. Estimated soil phosphorus conservation time for delayed P loading to lake given eight conformity cases and six soil sorption capacities (in each panel). Columns in each panel show P at the base of drain field (C_P in mg P/L), Soil adsorption capacity (q_ads in mg P/kg of substrate), Septic system effluent ($\boldsymbol{Q_{eff}}$ in L/d), and Soil conservation time from septic system to lake (($\boldsymbol{t_{conservation}}$ in yr), respectively

Given the average 2.3 habitants per household in the municipality of St-Hippolyte and that each person generates an average of 270 L/person/d of wastewater in Quebec, the calculated affluent rate is equal to 621 L/day per dwelling, which represents Q_{aff} as the inflow rate into the system. Q_{aff} is equal to Q_{eff}, only Q_{aff} is divided between underground and surface flows (Equations S4 through S7). Considering that the catchment is not habited all year long, the occupancy rate (40%) multiplies the influent (621 L/day/capita) and effluent flows to model hydraulic load reduction in the system since the system is not used at its full capacity, only for the

duration the residences are habited (40% of the time in historical conditions, 80% under changing anthropogenic conditions). Therefore, septic systems contribute between 248 and 210 L/d/capita in groundwater flow towards the lake. The variable V_{soil} was calculated based on depth, length, and width of the soil prism solicited for nutrient transport. The length corresponds to 15 m or 3 m distance from the lake. The depth is a calibration parameter representing the vertical leaching depth of 0.3 m of phosphorus in the unsaturated portion of the soil, and the width of the prism corresponds to the width of the drain field unit. According to local Q-2, r. 22 guidelines, the dimensions of the drain field varies based on the number of bedrooms in a dwelling, which dictates the required infiltration area (MDDELCC, 2015), as shown in Table S1.

Table S1. Minimum required drain field infiltration area according to number of bedrooms per household (MDDELCC, 2015)

Dwelling	**Daily flow (L/d)**	**Minimal infiltration available surface area (m^2)**
Number of bedrooms		
1	0-540	80
2	541-1080	120
3	1081-1620	180
5	2161-2700	300
6	2701-3240	360

However, as it is almost impossible to determine the number of bedrooms in each dwelling, an average infiltration width, representative of all building types, is determined. For this purpose, by knowing the minimum required infiltration area, dimensions were determined for each dwelling case in Table S1. Width for each residency case was divided by the average number of inhabitants per household, i.e., 2.3 to find the width required per person. An arithmetic mean was then conducted for each bedroom case, then another to determine the mean width required for all cases, resulting in an average width of 5.65 m/person for the drain field. By multiplying 5.65 m/person by 2.3, a width of 13 m for the drain field is obtained, which accounts for all possible dwelling scenarios. Finally, $t_{conservation}$ is computed using Equation S3. These soil conservation times are shown in Fig. S4. The conservation time is then compared to septic system age, which is provided by municipality officials in our study area to identify whether the groundwater is released towards

lake or not, yet at a given time step. Fig. S5 shows these septic system age categories and number of systems in each age category.

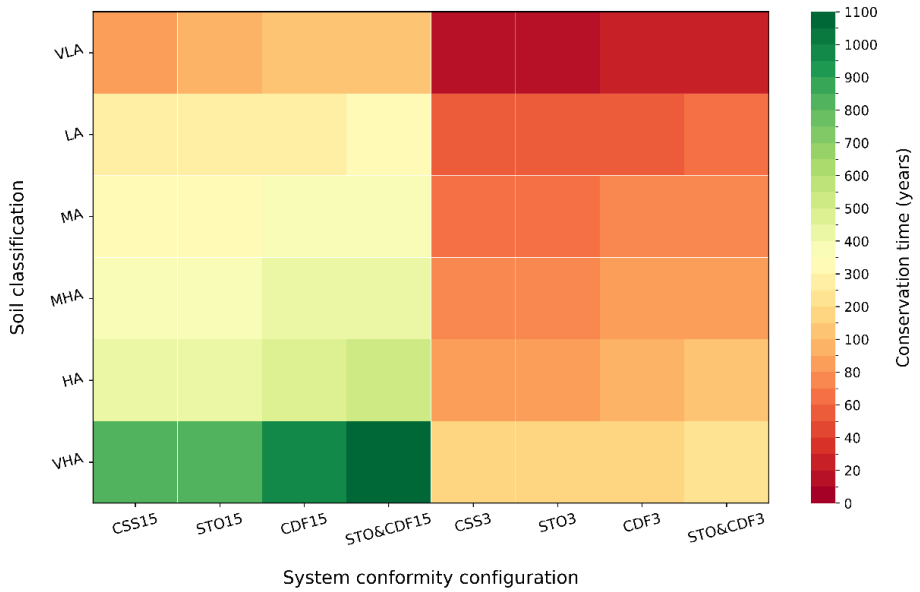

Fig. S4. Phosphorus conservation times as combinations of eight conformity cases (CSS15 to STO&CDF3) and six soil types (VLA to VHA) as computed by Equation S3

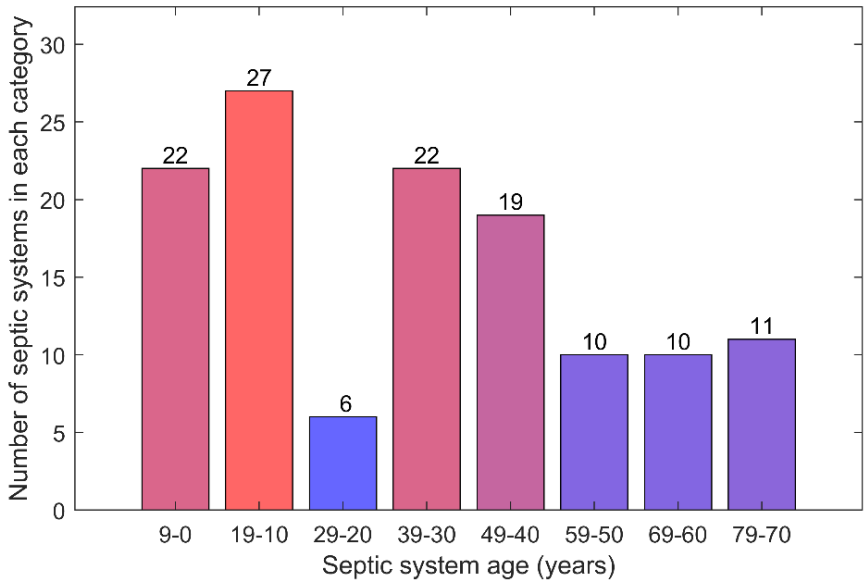

Fig. S5. Number of septic systems and their corresponding age category in the Lake *en Coeur* catchment area

S1.2. Total phosphorus export towards lake

The main phosphorus source in this study is from septic systems. Fig. S6 shows the elements either releasing (F) or retaining (C) phosphorus fluxes with red and green arrows, respectively. Conforming systems (CSS) do not generate any surface flow, hence they do not have F2 and F4 flows. STO15 and STO3 cases generate an F2 flow, CDF3 and CDF15 generate and F4 flow, and when they occur simultaneously, they generate a combination of both surface and groundwater flows. The septic system mass balance to estimate total phosphorus at the base of the drain field is given by Equations S4-S7:

$$F_{total} = F_{surface} + F_{underground} \tag{S4}$$

$$F_{surface}(or\ F6) = F2 + F4 - C3 \tag{S5}$$

$$F3 = F1 - F2 - C1 \tag{S6}$$

$$F_{underground}(or\ F5) = F3 - F4 - C2 \tag{S7}$$

This mass balance determines phosphorus concentration C_p at the base of the drain field generated by each conformity case to compute $t_{conservation}$ (Equation S3).

Some conformity cases generate more surface or underground phosphorus to be exported towards the lake. CSS15 generates the most underground phosphorus as there is no surface flow, and STO&CDF3 generates the highest surface flow, as shown in Fig. S6.

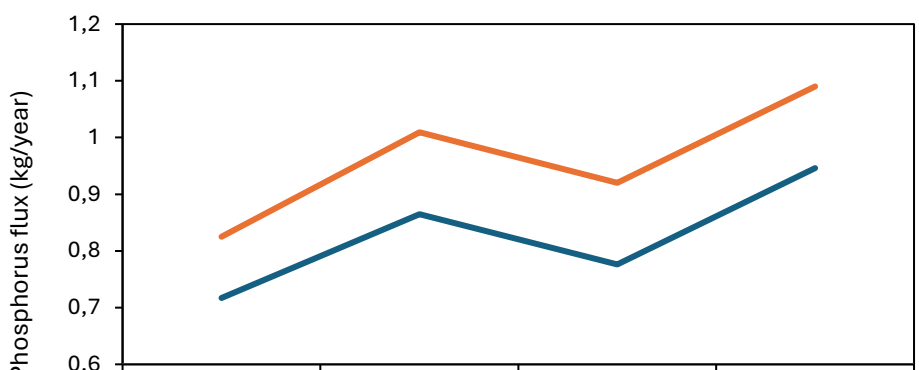

	CSS	STO	CDF	STO & CDF
AT 15 meter	0,717	0,865	0,776	0,946
AT 3 meter	0,825	1,009	0,92	1,09

Fig. S6 Phosphorus fluxes generated for eight conformity cases and distance from lake

S1.3 Other variables affecting lake water phosphorus and volume

Apart from septic systems, there are other anthropogenic sources of phosphorus to the lake, including the atmospheric deposition (P_{atm}) and forest contribution (P_{forest}). Equations S8 and S9 were applied to determine the annual phosphorus input from these two sources:

$$P_{atm} = C_{atm} \cdot A_{atm} \tag{S8}$$

$$P_{forest} = C_{forest} \cdot A_{forest} \tag{S9}$$

where C_{forest} is the export coefficient from forests (gP m^{-2} yr^{-1}), and A_{forest} the surface area of the forested zone on the watershed (m^2). The export coefficient of 0.0024 gP m^{-2} yr^{-1} for C_{forest} is assumed based on (Reckhow et al., 1980) and (Brylinsky, 2004) and a C_{atm} of 0.014 m^{-2} yr^{-1} was used based on (Tipping et al., 2014) and were calibrated accordingly. The forested surface area and the lake surface area were estimated using a QGIS software (Rosas-Chavoya et al., 2022).

A portion of the phosphorus in the lake is lost through the lake outflow ($P_{outflow}$), and another portion is lost through internal quality processes such as settling ($P_{settling}$). Lake sediments are often phosphorus sinks and play a crucial role in regulating nutrient metabolism (Pettersson, 1998). P settling is a complex phenomenon that needs to be modeled at much finer temporal resolution than the chosen annual scale and considering lake as a lumped entity. In this study both settling, also referred to as sedimentation, is considered as a calibration parameter, . All phosphorus sources from Equation 2 were multiplied by a settling coefficient that was optimized through Monte-Carlo realizations. A fraction of atmospheric inputs, forest contributions, and septic surface runoff was assumed to be particulate and therefore subject to settling, while the underground phosphorus fraction was assumed to be dissolved and not subject to settling. The settling coefficient represents this partitioning particulate and dissolved phosphorus. The coefficient that yielded median simulated concentrations closest to observation with the lowest absolute error was considered in the mass balance. The simulations yielded an optimal settling coefficient of 0.473.

Evapotranspiration from the watershed is found using the Hargreaves and Budyko equations as follows:

$$ET_0 = 0{,}0023 \cdot (T_{max} - T_{min})^{0{,}5} \cdot (T_{mean} + 17{,}8) \cdot R_a \tag{S10}$$

$$\frac{AET}{P} = \left[\frac{ET_0}{P} \cdot \tanh(\frac{ET_0}{P})^{-1} \cdot \ (1 - \exp(-\frac{ET_0}{P}))\right]^{0,5} \quad \text{(S11)}$$

where ET_0 (mm/d) is the reference evapotranspiration, T_{max} (˚C) the maximum daily temperature, T_{min}(˚C) the minimal daily temperature, T_{mean} the mean daily temperature, R_a (mm/d) the extraterrestrial radiation, AET is the actual evapotranspiration (mm/y), and P the yearly precipitation rate (mm/y). Precipitation in mm is obtained from the closest climate.

Lake evaporation rate is computed using Meyer's formula.

$$Ev = \ K_M \cdot (e_w - e_a) \cdot (1 + \frac{u_9}{16}) \quad \text{(S12)}$$

where K_M is a constant with a value of 0.50 assuming a smaller, and more shallow lake, e_w saturated vapor pressure at the lake's surface (mmHg), e_a air vapor pressure at lake's surface (mmHg), and u_9 monthly mean wind speed at 9 meters above ground surface (km/h).

S1.4. Monte Carlo sampling

While septic system conformity case and soil types are known for the watershed, their spatial location is unknown, due to confidentiality issues. These two variables were assumed random and follow a categorical distribution, indicated in Equations 4 and 5 in the article. These categories are determined with some prior knowledge thanks to the septic system inspection program carried out in the region. It was assumed that 80% of septic system are conform i.e., belong to CSS15 case or on other words, 80% septic systems have a chance of full conformity. The rest of conformity cases were assigned an equivalent probability of 2.9% because of the lack of prior knowledge on other types of system compliance. The model will then sample a random number as R ~ U [0,1] to determine which case the system will be attributed. If the randomly drawn number is equal to 0,35 for example, the system will be assigned CSS15 since the number belongs within the case's interval probability (see Table S2). If the drawn number is equal to 0.99, the system's conformity will be labeled as STO&CDF3. The same logic is applied for soil types. While we are aware of soil type locations, and number of septic systems in each zone, the specific septic systems located in these zones is unknown since the systems are not spatially bound in this model. Therefore, probability occurrences are allocated for these soil types as well (see Table S3).

Table S2. Conformity cases categories and the cumulative weighted probability of occurrence

Conformity categories	Probability of occurrence
CSS15	[0, 0.80]
STO15	[0.80, 0.83]
CDF15	[0.83, 0.86]
STO&CDF15	[0.86, 0.89]
CSS3	[0.89, 0.91]
STO3	[0.91, 0.94]
CDF3	[0.94, 0.97]
STO&CDF3	[0.97, 1.0]

Table S3. Soil type categories and the cumulative weighted probability of occurrence

Soil type categories	Probability of occurrence
VLA	[0, 0.20]
LA	[0.20, 0.39]
MLA	[0.39, 0.48]
MA	[0.48, 0.64]
HA	[0.64, 0.82]
VHA	[0.82, 1.0]

S2. Other supplementary tables and figures

Table S4. List of climate models from the CMIP6 and their specifications (Tebaldi et al., 2021)

Institution	Model(s)	Model information	Experiments used in the study
Beijing Climate Center (China)	BCC-CSM2-MR	(Wu et al., 2021)	historical, SSPs 245 & 585
Canadian Centre for Climate Modelling and Analysis (Canada)	CanESM5	(Swart et al., 2019)	historical, SSPs 245 & 585
Institute for Numerical Mathematic (Russia)	INM-CM5.0; INM-CM4.8	(Volodin et al., 2017; Volodin et al., 2018)	historical, SSPs 245 & 585
Institute of Atmospheric Physics (China)	FGOALS-g3	(Pu et al., 2020)	historical, SSPs 245 & 585
Korea Institute of Ocean Science and Technology	KIOST-ESM	(Pak et al., 2021)	historical, SSPs 245 & 585
NOAA – Geophysical Fluid Dynamics Laboratory (USA)	GFDL-ESM4	(Dunne et al., 2020)	historical, SSPs 245 & 585
Norwegian Climate Center (Norway)	NorESM2-LM; NorESM2-MM	(Seland et al., 2020); (Tjiputra et al., 2020)	historical, SSPs 245 & 585
National Center for Atmospheric Research (Taiwan)	TaiEMS1	(Lee et al., 2020)	historical, SSPs 245 & 585
The Euro-Mediterranean Centre on Climate Change (Italy)	CMCC-ESM2	(Lovato et al., 2022)	historical, SSPs 245 & 585

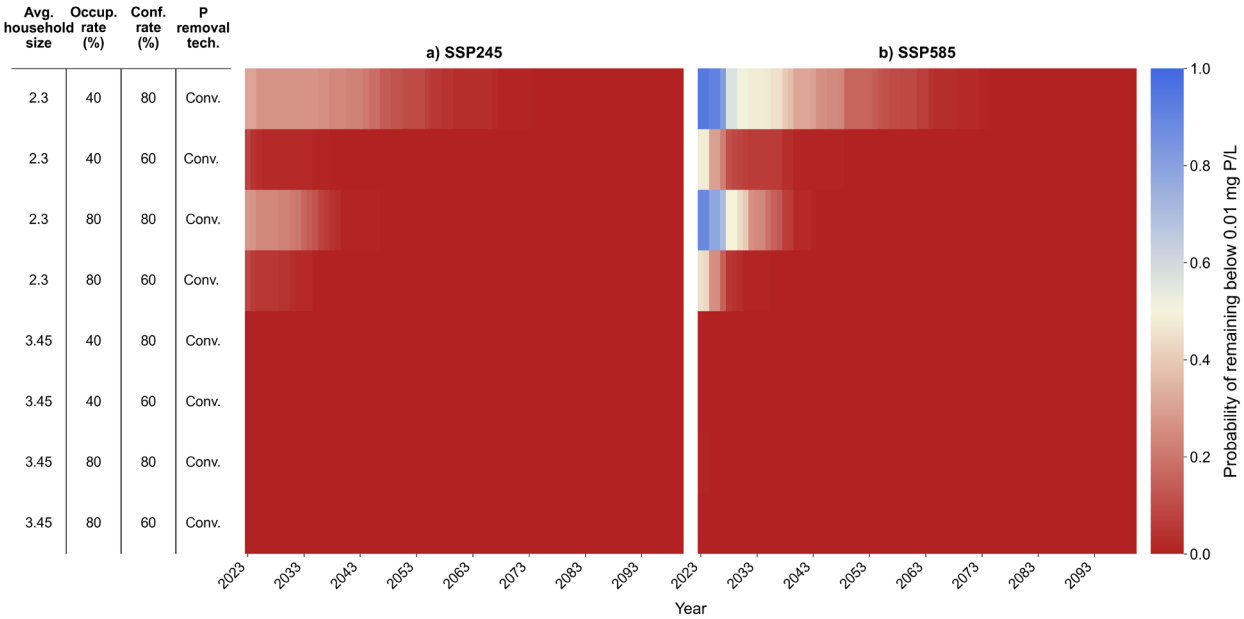

Fig. S7. Survival probability of 0.01 mg P/L meso-eutrophic per anthropogenic scenario with conventional P removal technology under SSP2-4.5 and SSP5-8.5 for future period of 2023-2100 using the Kaplan-Meier method

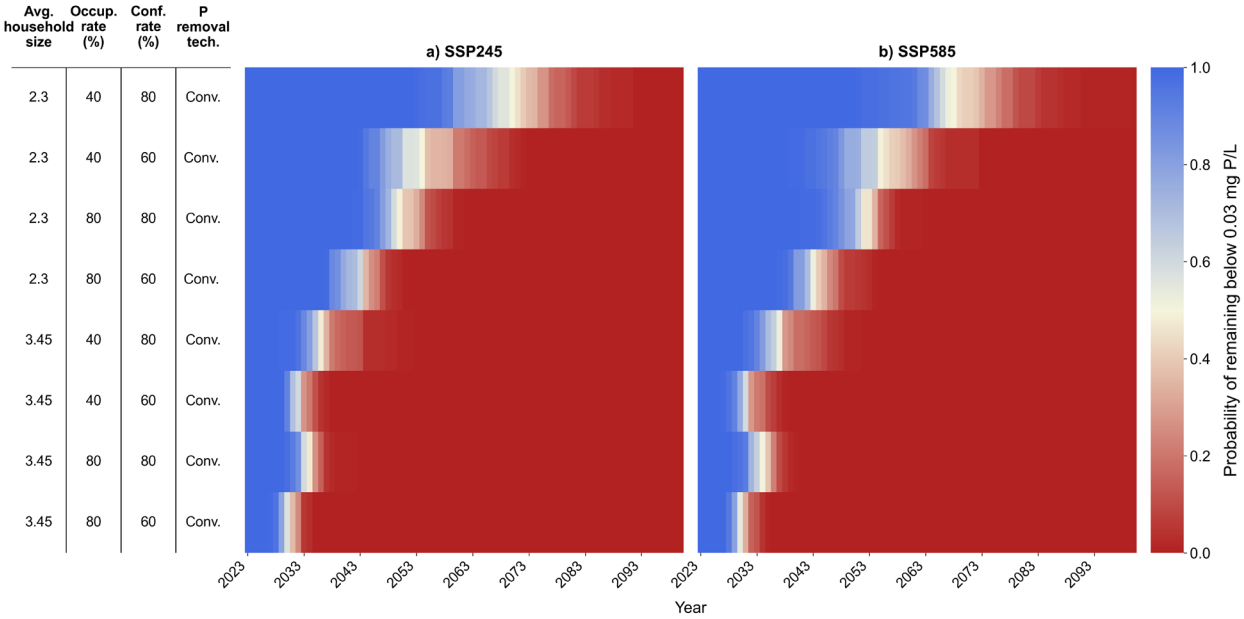

Fig. S8. Survival probability of 0.03 mg P/L eutrophic per anthropogenic scenario with conventional P removal technology under SSP2-4.5 and SSP5-8.5 for future period of 2023-2100 using the Kaplan-Meier method

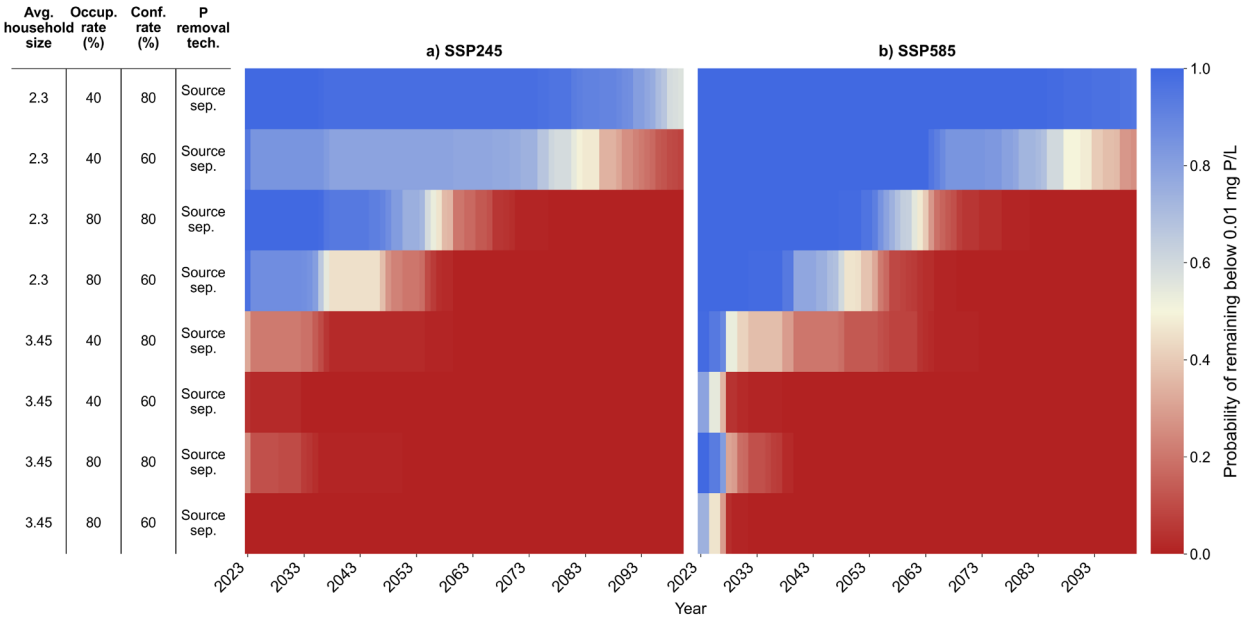

Fig. S9. Survival probability of 0.01 mg P/L meso-eutrophic per anthropogenic scenario with source separation technology under SSP2-4.5 and SSP5-8.5 for future period of 2023-2100 using the Kaplan-Meier method

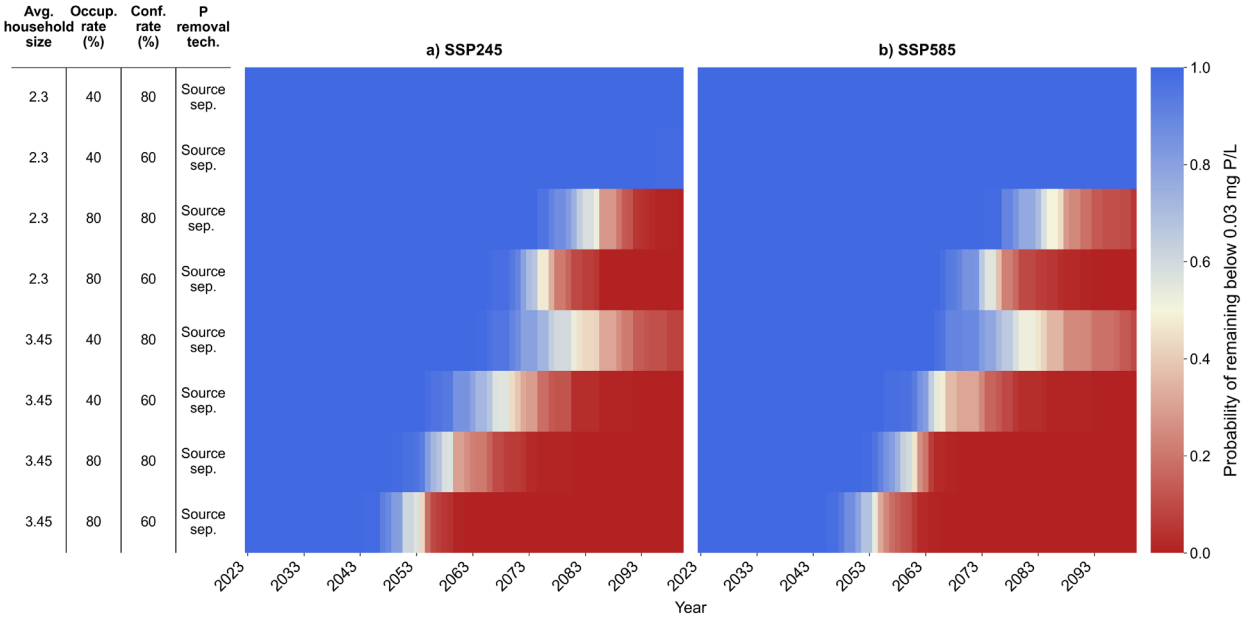

Fig. S10. Survival probability of 0.03 mg P/L eutrophic per anthropogenic scenario with source separation technology under SSP2-4.5 and SSP5-8.5 for future period of 2023-2100 using the Kaplan-Meier method

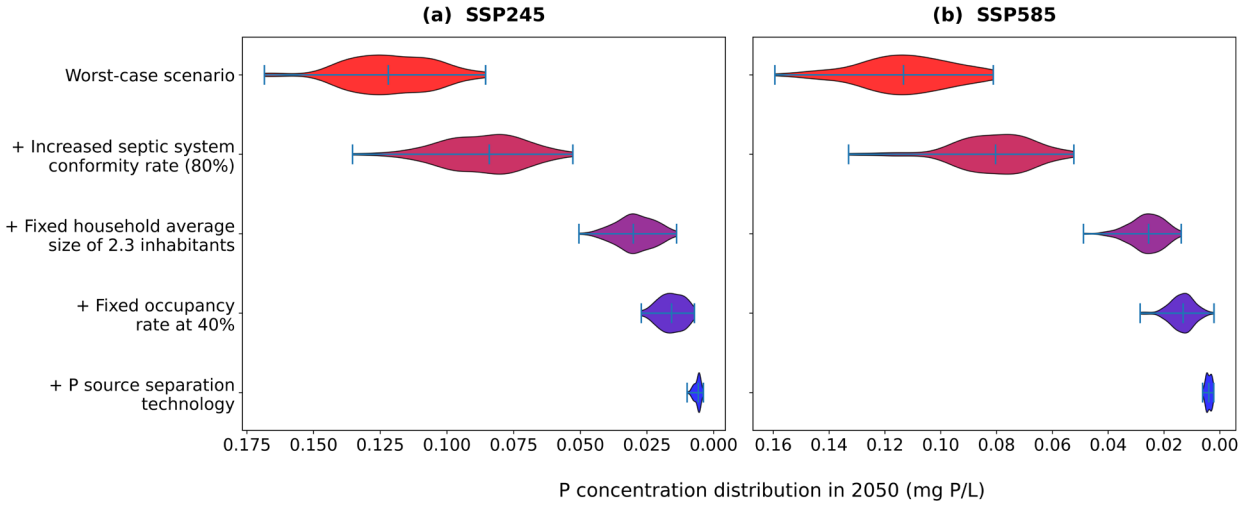

Fig. S11. Evolution of the median phosphorus concentration with the gradual implementation of mitigation strategies by 2050 under SSP2-4.5 and SSP5-855 for the future period 2023-2100

References

Brylinsky, M., 2004. User's Manual for Prediction of Phosphorus Concentration in Nova Scotia Lakes: A Tool for Decision Making. Acadia University.

Dunne, J.P., Horowitz, L.W., Adcroft, A.J., Ginoux, P., Held, I.M., John, J.G., et al., 2020. The GFDL Earth System Model version 4.1 (GFDL-ESM 4.1): overall coupled model description and simulation characteristics. J. Adv. Model. Earth Syst. 12 (11), e2019MS002015.

Lee, W.L., Wang, Y.C., Shiu, C.J., Tsai, I., Tu, C.Y., Lan, Y.Y., et al., 2020. Taiwan Earth System Model version 1: description and evaluation of mean state. Geosci. Model Dev. 13 (9), 3887–3904.

Lovato, T., Peano, D., Butenschön, M., Materia, S., Iovino, D., Scoccimarro, E., et al., 2022. CMIP6 simulations with the CMCC Earth System Model (CMCC-ESM2). J. Adv. Model. Earth Syst. 14 (3).

MDDELCC, 2015. Isolated Dwellings Wastewater Treatment. Government of Quebec.

Pak, G., Noh, Y., Lee, M.-I., Yeh, S.-W., Kim, D., Kim, S.-Y., et al., 2021. Korea Institute of Ocean Science and Technology Earth System Model and its simulation characteristics. Ocean Sci. J. 56 (1), 18–45.

Pettersson, K., 1998. Mechanisms for internal loading of phosphorus in lakes. Hydrobiologia 373, 12–25.

Pu, Y., Liu, H., Yan, R., Yang, H., Xia, K., Li, Y., et al., 2020. CAS FGOALS-g3 model datasets for the CMIP6 Scenario Model Intercomparison Project (ScenarioMIP). Adv. Atmos. Sci. 37 (10), 1081–1092.

Reckhow, K.H., Beaulac, M.W., Simpson, J.T., 1980. Modeling Phosphorus Loading and Lake Response under Uncertainty: A Manual and Compilation Export Coefficients. Michigan State University.

Rosas-Chavoya, M., Gallardo-Salazar, J.L., López-Serrano, P.M., Alcántara-Concepión, P.C., León-Miranada, A.K., 2022. QGIS a constantly growing free and open-source geospatial software contributing to scientific development. Cuad. Investig. Geogr. 48, 197–213.

Seland, Ø., Bentsen, M., Olivié, D., Toniazzo, T., Gjermundsen, A., Graff, L.S., et al., 2020. Overview of the Norwegian Earth System Model (NorESM2) and key climate response of CMIP6 DECK, historical, and scenario simulations. Geosci. Model Dev. 13 (12), 6165–6200.

Swart, N.C., Cole, J.N.S., Kharin, V.V., Lazare, M., Scinocca, J.F., Gillett, N.P., et al., 2019. The Canadian Earth System Model version 5 (CanESM5.0.3). Geosci. Model Dev. 12 (11), 4823–4873.

Tebaldi, C., Debeire, K., Eyring, V., Fischer, E., Fyfe, J., Friedlingstein, P., et al., 2021. Climate model projections from the Scenario Model Intercomparison Project (ScenarioMIP) of CMIP6. Earth Syst. Dynam. 12 (1), 253–293.

Tipping, E., Benham, S., Boyle, J.F., Crow, P., Davies, J., Fischer, U., et al., 2014. Atmospheric deposition of phosphorus to land and freshwater. Environ. Sci.: Process. Impacts 16, 1608–1617.

Tjiputra, J.F., Schwinger, J., Bentsen, M., Morée, A.L., Gao, S., Bethke, I., et al., 2020. Ocean biogeochemistry in the Norwegian Earth System Model version 2 (NorESM2). Geosci. Model Dev. 13 (5), 2393–2431.

Volodin, E.M., Mortikov, E.V., Kostrykin, S.V., Galin, V.Y., Lykossov, V.N., Gritsun, A.S., et al., 2017. Simulation of the present-day climate with the climate model INMCM5. Clim. Dyn. 49 (11), 3715–3734.

Volodin, E.M., Mortikov, E.V., Kostrykin, S.V., Galin, V.Y., Lykossov, V.N., Gritsun, A.S., et al., 2018. Simulation of the modern climate using the INM-CM48 climate model. Russ. J. Numer. Anal. Math. Model. 33 (6), 367–374.

Wu, T., Yu, R., Lu, Y., Jie, W., Fang, Y., Zhang, J., et al., 2021. BCC-CSM2-HR: a high-resolution version of the Beijing Climate Center Climate System Model. Geosci. Model Dev. 14 (5), 2977–3006.